Original Article

MOLECULAR METABOLISM

Pharmacological inhibition of ALCAT1 mitigates amyotrophic lateral sclerosis by attenuating SOD1 protein aggregation

Xueling Liu [1,2], Jun Zhang [2], Jie Li [1], Chengjie Song [1], Yuguang Shi [1,2,*]

ABSTRACT

Objective: Mutations in the copper-zinc superoxide dismutase (*SOD1*) gene cause familial amyotrophic lateral sclerosis (ALS), a progressive fatal neuromuscular disease characterized by motor neurons death and severe skeletal muscle degeneration. However, there is no effective treatment for this debilitating disease, since the underlying cause for the pathogenesis remains poorly understood. Here, we investigated a role of acyl-CoA:lysocardiolipin acyltransferase 1 (ALCAT1), an acyltransferase that promotes mitochondrial dysfunction in age-related diseases by catalyzing pathological remodeling of cardiolipin, in promoting the development of ALS in the $SOD1^{G93A}$ transgenic mice.

Methods: Using $SOD1^{G93A}$ transgenic mice with targeted deletion of the *ALCAT1* gene and treated with Dafaglitapin (Dafa), a very potent and highly selective ALCAT1 inhibitor, we determined whether ablation or pharmaceutical inhibition of ALCAT1 by Dafa would mitigate ALS and the underlying pathogenesis by preventing pathological remodeling of cardiolipin, oxidative stress, and mitochondrial dysfunction by multiple approaches, including lifespan analysis, behavioral tests, morphological and functional analysis of skeletal muscle, electron microscopic and Seahorse analysis of mitochondrial morphology and respiration, western blot analysis of the $SOD1^{G93A}$ protein aggregation, and lipidomic analysis of cardiolipin content and acyl composition in mice spinal cord.

Results: ALCAT1 protein expression is potently upregulated in the skeletal muscle of the $SOD1^{G93A}$ mice. Consequently, ablation or pharmacological inhibition of ALCAT1 by Dafa attenuates motor neuron dysfunction, neuronal inflammation, and skeletal muscle atrophy in $SOD1^{G93A}$ mice by preventing $SOD1^{G93A}$ protein aggregation, mitochondrial dysfunction, and pathological CL remodeling, leading to moderate extension of lifespan in the $SOD1^{G93A}$ transgenic mice.

Conclusions: ALCAT1 promotes the development of ALS by linking $SOD1^{G93A}$ protein aggregation to mitochondrial dysfunction, implicating Dafa as a potential treatment for this debilitating disorder.

Keywords ALS; Cardiolipin; Mitochondrial dysfunction; Neuronal inflammation; SOD1 aggregation

1. INTRODUCTION

Amyotrophic lateral sclerosis (ALS), also known as Lou Gehrig's disease, is a motor neuron disease in adults, and is the third most common neurodegenerative disease after Alzheimer's disease (AD) and Parkinson's disease (PD) [1,2]. ALS mainly affects the upper and lower motor neurons, which causes progressive muscle weakness and atrophy, paralysis, and ultimately death due to respiratory failure within 2–5 years of symptom onset [3,4]. Although two drugs, including anti-glutamatergic agent Riluzole and antioxidant Edaravone have been approved by Food and Drug Administration (FDA) for the treatment of ALS in patients, their efficacies are quite poor in clinical trials [5,6]. There are no other effective treatments for ALS to date, because the molecular mechanisms underlying the pathogenesis remain largely unknown. Mutations in copper-zinc superoxide dismutase (*SOD1*) are the first identified genetic defect that causes familial ALS [7]. ALS-associated mutations in the *SOD1* gene cause SOD1 protein misfolding and aggregation, leading to motor neurons degeneration and death [8]. Additionally, mutant SOD1 aggregates at the mitochondrial membrane space of motor neurons, leading to mitochondrial damage and dysfunction, which is a central feature of the pathogenesis in ALS [9,10]. However, neither the underlying causes of SOD1 aggregation nor its effect on mitochondrial dysfunction are well understood, which has prevented the development of targeted and more effective treatment for this debilitating disorder.

Cardiolipin (CL) is a mitochondrial signature phospholipid that is required for mitochondrial membrane structure, oxidative phosphorylation, ATP production, mtDNA biogenesis, and mitochondrial quality control [11–15]. CL is remodeled after initial biosynthesis into its matured form that is enriched with linolic acid, known as tetra-linoleoyl CL (TLCL), which is required for optimal mitochondrial function in metabolic tissues, such as heart, skeletal muscle, and liver [16–20].

[1]Department of Biochemistry and Molecular Biology, School of Basic Medical Sciences, Nanjing Medical University, Nanjing, China [2]Sam and Ann Barshop Institute for Longevity and Aging Studies, Department of Pharmacology, University of Texas Health Science Center at San Antonio, San Antonio, TX 78229, USA

*Corresponding author. Joe R. & Teresa Lozano Long Distinguished Chair in Metabolic Biology, Barshop Institute for Longevity and Aging Studies, University of Texas Health Science Center at San Antonio, 4939 Charles Katz Dr., San Antonio, TX, 78229, USA. Fax: +210 562 6150. E-mail: shiy4@uthscsa.edu (Y. Shi).

Received April 29, 2022 • Revision received June 20, 2022 • Accepted June 22, 2022 • Available online 28 June 2022

https://doi.org/10.1016/j.molmet.2022.101536

Due to its high content in polyunsaturated fatty acids and exclusive location in mitochondrial membrane where reactive oxygen species (ROS) are generated, CL is highly sensitive to oxidative damage of its four fatty acyl chains by ROS [15,21]. Defective CL remodeling leads to Barth syndrome [22,23], and is also implicated in the pathogenesis of various age-related metabolic disorders, including obesity [24], cardiovascular diseases [15,18,25], fatty liver disease [26], and PD [27–29]. Lipidomic analysis revealed a significant decrease of CL content in the spinal cord of transgenic rat expressing the *SOD1*^{G93A} mutant, a rat model of ALS [30]. In addition, CL peroxidation was increased in the spinal cord and brain of the *SOD1*^{G93A} transgenic mice, which is accompanied by impaired mitochondrial oxidative phosphorylation activity and increased cytochrome c release, a leading indicator of apoptosis [31]. These alterations in CL are consistent with the loss of mitochondrial integrity observed in several models of ALS [32]. However, the underlying causes of aberrant CL metabolism in ALS remain elusive.

ALCAT1 is an acyltransferase that catalyzes reacylation of lysocardiolpin using acyl-CoA as the acyl donor, a key step in CL remodeling [33]. Our recent work show that upregulation of ALCAT1 expression by reactive oxygen species (ROS) promotes mitochondrial dysfunction by catalyzing pathological remodeling of CL with long chain polyunsaturated fatty acids, such as docosahexaenoic acid (DHA) [24]. Enrichment of DHA further exacerbates oxidative damage of CL by ROS, leading to CL peroxidation and mitochondrial dysfunction [24]. Consequently, ablation of ALCAT1 effectively protected mice from the development of various age-related diseases, including obesity, type 2 diabetes, fatty liver disease, cardiomyopathy, heart failure, and PD [18,24–26,29]. Moreover, CL remodeling by ALCAT1 also leads to multiple metabolic defects that are highly reminiscent of those observed in ALS, including CL depletion and peroxidation, oxidative stress, and mitochondrial dysfunction [30,31]. However, it remains to be determined whether CL remodeling by ALCAT1 also plays a role in the pathogenesis of ALS. Using mice with transgenic expression of the *SOD1*^{G93A} as a mouse model of ALS, we investigated a role of ALCAT1 in regulating the onset and development of ALS. We show that upregulated ALCAT1 by the SOD1^{G93A} protein aggregation is implicated in the pathogenesis of the ALS mice. Accordingly, ablation or pharmacological inhibition of the ALCAT1 attenuated motor neuron loss, skeletal muscle atrophy, and neuroinflammation, resulting in moderate delay in disease onset, improvement in motor function, and extension of lifespan of the *SOD1*^{G93A} mice. These findings identified ALCAT1 as a missing link between *SOD1*^{G93A} protein aggregation and the development of ALS.

2. MATERIALS AND METHODS

2.1. Reagents

Antibodies used in the studies included polyclonal antibodies to NLRP3 (D4D8T), GFAP (E4L7M), IBA1 (E404W), all of which were purchased from Cell Signaling Technology. Monoclonal anti-β-actin (A5441) antibody was from Sigma–Aldrich. HRP conjugated goat anti-mouse IgG secondary antibody (31,430) and HRP conjugated goat anti-rabbit IgG secondary antibody (31,463) were purchased from Thermo Fisher Scientific. Phosphatase inhibitor cocktail (P5726) was purchased from Millipore Sigma. EDTA-free protease inhibitor cocktail (11,873,580,001) was from Roche. Wheat germ agglutinin (W488) was from Life Technologies and 10% fetal bovine serum (S11550H) was from Atlanta Biologicals. CRISPR/Cas9 plasmids (sc-432,509 and sc-432509-HDR) were from Santa Cruz. Viafect transfection regent (E4982) was obtained from Promega. Hoechst 33,342 solution (62,249), H_2DCFDA (D399), SuperScript™ IV first strand synthesis system (18,091,200), TRIzol (15,596,018), RNaseOUT inhibitor (10,777–019), Oligo_dT (18,418–12), SYBR™ green PCR master mix (4,309,155) and penicillin/streptomycin (15,140,122) were from Thermo Fisher Scientific. The pF141 pAcGFP1-SOD1_WT (26,402) and pF145 pAcGFP1-SOD1_G93A (26,406) plasmids were purchased from Addgene. Dafaglitapin (ALCAT1 inhibitor) was obtained from Perenna Pharmaceuticals Inc. (San Antonio, TX, USA). ALCAT1 antibody was kindly provided by Dr. Hiroyuki Arai of Tokyo, Japan.

2.2. Mice care

High-copy *SOD1*^{G93A} transgenic mice (B6.Cg-Tg(SOD1*G93A)1Gur/J) were obtained from the Jackson Laboratory (Strain#: 004435). The *SOD1*^{G93A} mice with target deletion of ALCAT1 (*SOD1*^{G93A}/*ALCAT1*$^{-/-}$) were generated by mating the *SOD1*^{G93A} mice with the global *ALCAT1* gene knockout mice (*ALCAT1*$^{-/-}$) previously generated by us [24]. All animals were maintained in an environmentally controlled facility with a diurnal light cycle and free access to water and a standard rodent chow. All experiments involving animals were approved by the Institutional Animal Care and Use Committee, and use protocols according to NIH guidelines (NIH publication no.86–23 [1985]).

2.3. Animal survival and behavioral studies

Disease onset and survival analyses were performed using Kaplan–Meier analyses. Endpoint was defined as the death point when mice could no longer regain their upright position within 30 s after being placed on their back. Disease onset was determined when the mice already showed dragging feet/knuckles. Paralysis was defined when the mice showed single leg paralysis as previous described [34]. Behavioral measurements, including grip strength test and rotarod test, were performed in a blinded manner, and were carried out in male mice at the age of 120 days. *Grip strength*: Mice are lifted over the baseplate by the tail so that its forelimbs and hind limbs are allowed to grasp onto the steel grip. The operator gently pulls backwards until the grip is released. The peak amount of force required to make the mouse release its grip on the apparatus was sensed by the instrument. *Rotarod test:* The mice were trained until they could remain on the rotarod for 120 s without falling before testing. During testing, mice were placed on the rotarod, and the rotation speed was increased from 5 to 40 r/min over 5 min. The latency (time) to fall from the rotarod was automatically recorded. Each mouse was tested in three independent trials with a 20 min intertrial interval. The latency to fall was calculated as the average of three trials.

2.4. Histological analysis

Isoflurane was used to anesthetize the animals before the animals were sacrificed. The lumbar spinal cord and muscle tissue were collected and fixed in 4% paraformaldehyde solution at 4 °C for 24 h. Fixed tissues were dehydrated and embedded in paraffin, and 5 μm sections were cut with a Leica RM-2162 (Leica, Bensheim, Germany). H&E staining was performed as previously described [18]. WGA (5 μg/mL, Thermo Fisher Scientific) staining was performed in the muscle sections by using Alexa Fluor 488 conjugate dye. For immunofluorescence staining, the lumbar spinal cord sections were washed three times with 0.3% Triton X-100 in PBS, blocked with 5% BSA for 60 min at room temperature and then incubated with anti-IBA1 (1:200, CST, E404W) antibody or anti-GFAP (1:200, CST, E4L7M) antibody at 4 °C for 24 h. Sections were washed (3 × 5 min) in PBST (PBS containing 1% tween-20) in the next day and incubated with goat anti-rabbit IgG secondary antibody conjugated to FITC for 2 h at room temperature in the dark. Finally, sections were washed and stained with DAPI, then

mounted using mounting medium and imaged using a laser confocal fluorescent microscope. ImageJ was used to assess the extent of immunoreactivity for GFAP and IBA1. Same intensity threshold was applied to all images to include the positive labeling while minimizing the inclusion of nonspecific background staining.

2.5. Cell culture and generation of *ALCAT1* gene knockout NSC-34 cells using CRISPR/Cas9 gene editing

An NSC-34 murine motor neuron cell line was purchased from CEDARLANE Corporation (Burlington, Canada). Cells were cultured in Dulbecco's modified Eagle medium (DMEM) with 10% fetal bovine serum (FBS), 1% penicillin, and streptomycin and maintained in 95% air plus 5% CO2 at 37 °C. *ALCAT1* gene was knocked out in NSC-34 cells by transfecting *CRISPR/Cas9* mouse plasmid from Santa Cruz Biotechnology (sc-432,509 and sc-432509-HDR) using Viafect transfection regent (Promega, E4982), and then purified through green fluorescent protein and red fluorescent protein at the UT Health San Antonio Flow Cytometry Core. Cells were kept under selection with 2 μg/mL puromycin (San Cruz Biotechnology, sc-205821).

2.6. Quantitative real time-PCR (qRT-PCR) analysis

Total RNA was extracted from mice muscle or spinal cord tissues using TRIzol reagent, and RNA quantity was determined at 260 nm (NanoDrop 1000 Spectrometer; Thermal Scientific). Single stranded cDNA was synthesized using SuperScript IV reverse transcriptase system, and gene expression was determined by qRT-PCR, which was performed by using SYBR green PCR master mix and the 7300 Real-Time PCR System (Applied Biosystems, Waltham, MA, USA). The mRNA levels were determined using a standard curve method and normalized to the level of *Gapdh* which were used as internal standards. The primers used in PCR are shown below:

TNF1α: Forward, 5′-CCCTCACACTCAGATCATCTTCT-3′
Reverse, 5′-GCTACGACGTGGGCTACAG-3′
IL-1β: Forward, 5′-GACCTTCCAGGATGAGGACA-3′
Reverse, 5′-AGGCCACAGGTATTTTGTCG-3′
Gapdh: Forward, 5′-AATGGTGAAGGTCGGTGTG-3′
Reverse, 5′-GTGGAGTCATACTGGAACATGTAG-3′

2.7. Transmission electron microscopy

Mitochondrial ultrastructure in mice muscle and spinal cord were evaluated by using electron microscopy (EM). Spinal cord or muscle were taken at the same site from three age- and sex-matched mice in each group to prepare slides and fixed in 5% glutaraldehyde and 4% paraformaldehyde in 0.1 M sodium cacodylate buffer (pH 7.4) with 0.05% $CaCl_2$ for 24 h. After washing in 0.1 M sodium cacodylate buffer, tissues were post-fixed in 1% OsO4 and 0.1 M cacodylate buffer overnight, dehydrated, and embedded in EMbed-812 resin. The sections were stained with 2% uranyl acetate, followed by 0.4% lead citrate, and viewed with a JEOL JEM-2200FS 200 kV electron microscope (Electron Microscopy Sciences Core at the University of Texas Health Science Center at San Antonio).

2.8. Oxygen consumption rate (OCR) measurement

OCR was measured using a Seahorse XF24 analyzer (Seahorse Bioscience, North Billerica, MA, USA). OCR in isolated mitochondria from frozen heart samples was analyzed using the same method as previously described [23,35]. In brief, an equal amount of mitochondria (20 μg protein/well) isolated from frozen spinal cord samples was loaded to XF24 microplate, and the OCR was then measured in response to the treatment with a mixture of succinate (5 mM) and rotenone (2 μM), antimycin A (4 μM), a mixture of TMPD (0.5 mM) and ascorbate (1 mM), and sodium azide (50 mM). Real-time OCR was recorded two times during each conditional cycle.

2.9. Lipidomic analysis

The lipidomic analysis was carried out using methods previously described [24]. Briefly, total lipids extracted from the spinal cord of mice at the age of 120 days were analyzed by triple-quadruple mass spectrometer (MS) (Thermo Electron TSQ Quantum Ultra) controlled by Xcalibur system software. All the MS spectra and tandem MS spectra were automatically acquired by a customized sequence subroutine operated under Xcalibur software.

2.10. Cell treatment and analysis of ROS production

NSC-34 cells transiently expressed either the WT SOD1 or the $SOD1^{G93A}$ mutant were pre-exposed to different concentration of Dafa for 2 h, followed by treatment with H_2O_2 (200 μM) and Dafa for another 3 h, and then processed for further analysis. The ROS generation in NSC-34 cells was investigated by using 2′,7′-dichlordehydrofluorescein-diacetate (DCFH-DA; Molecular Probes) at a final concentration of 5 μM as previously described [36]. Cells were incubated with dye in culture medium in the dark for 30 min at 37 °C, and then harvested with 0.05% trypsin—EDTA solution, suspended in a fresh medium, and immediately analyzed.

2.11. Detection of SOD1 protein aggregation

To assay the $SOD1^{G93A}$ aggregation, spinal cord homogenates from mice and NSC-34 transfected cells was prepared as described [37]. Briefly, spinal cord or cells were sonicated in 0.5% Nonidet P-40 lysis (50 mM Tris—HCl (PH 8.0), 150 mM NaCl, 0.5% NP-40, 5 mM EDTA and a protease inhibitor cocktail 1:100 dilution). Tissue or cell lysates were spun down at 100,000 g for 15 min at 4 °C. Insoluble fraction was resuspended in loading buffer without β-mercaptoethanol.

2.12. Statistical analysis

Data were analyzed using GraphPad Prism software (version 6.0) and represented as mean ± SD. Two-way or one-way ANOVA followed by Bonferroni post hoc tests were utilized for multiple group comparisons. Student's t-test was used for comparisons between two groups. Statistical differences on mice survival rate, disease onset and paralysis were done by Log-rank (Mantel—Cox) test. Statistical significance was considered at $^{*}p < 0.05$, $^{**}p < 0.01$, $^{***}p < 0.001$.

3. RESULTS

3.1. Ablation or pharmacological inhibition of ALCAT1 delays the onset of ALS, leading to significant extension of lifespan in the $SOD1^{G93A}$ mice

Upregulated ALCAT1 expression was implicated in the pathogenesis of PD and several other age-related metabolic diseases by catalyzing pathological remodeling of CL [15,18,21,24–26,29]. Using the male $SOD1^{G93A}$ transgenic mice with targeted deletion of the *ALCAT1* gene ($SOD1^{G93A}/ALCAT1^{-/-}$), we investigated the role of ALCAT1 in the onset and development of ALS disease. The $SOD1^{G93A}/ALCAT1^{-/-}$ mice were generated by crossing the $SOD1^{G93A}$ mice with the global *ALCAT1* gene knockout mice ($ALCAT1^{-/-}$) previously generated by us [24]. As shown in Figure 1A, ALCAT1 deficiency moderately prolonged the lifespan of the $SOD1^{G93A}$ mice (Figure 1A, quantified in Figure 1B). Consistently, ablation of ALCAT1 also delayed disease progression, as evidenced by a moderate delay in disease onset (Figure 1C, quantified in Figure 1D) and paralysis in the $SOD1^{G93A}/ALCAT1^{-/-}$ mice relative to the $SOD1^{G93A}$ mice (Figure 1E, quantified in Figure 1F).

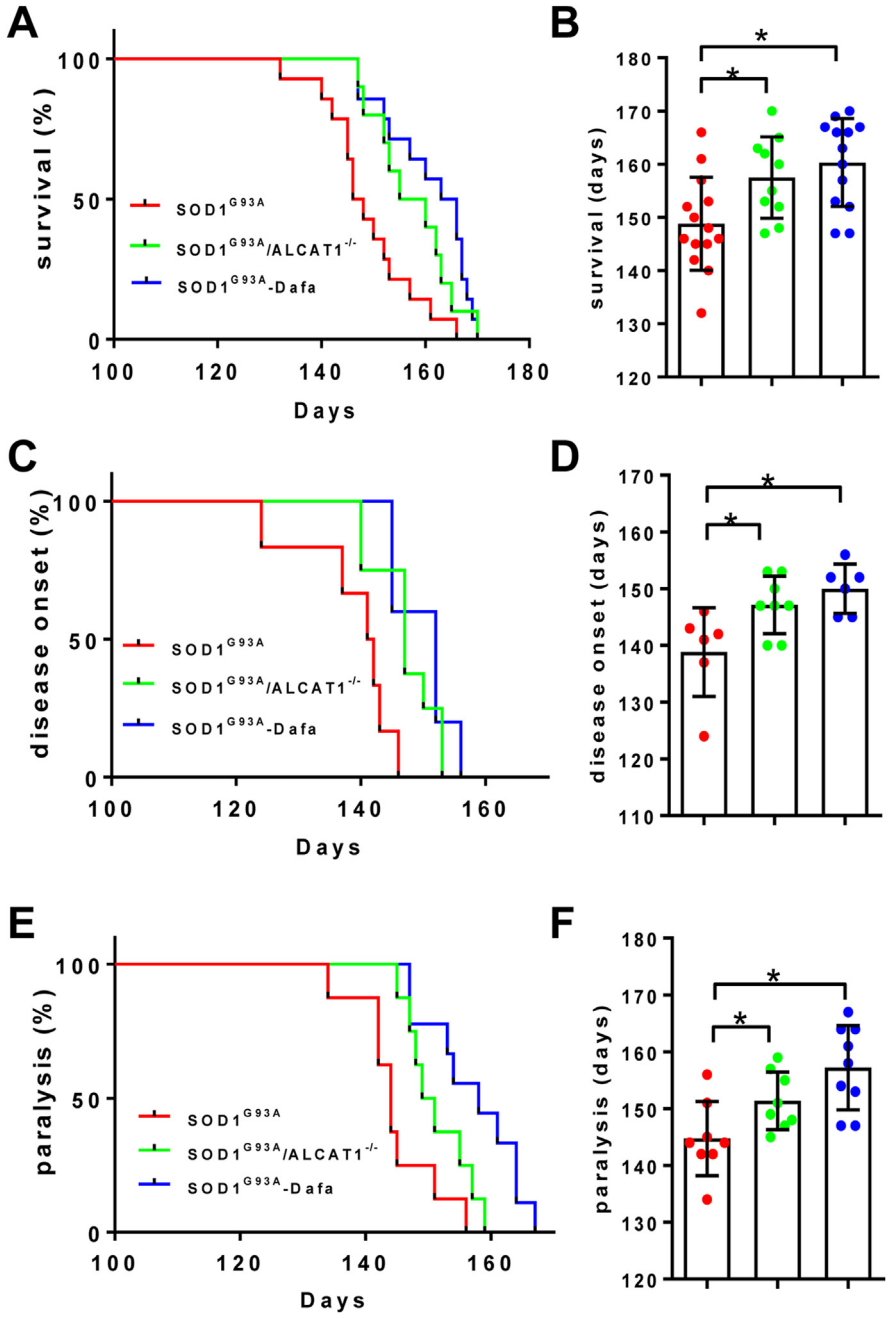

Figure 1: ALCAT1 deficiency or inhibition by Dafa extends lifespan by slowing disease progression in the *SOD1^{G93A}* mice. (**A**) Kaplan–Meier cumulative survival curve of the *SOD1^{G93A}*, *SOD1^{G93A}/ALCAT1$^{-/-}$*, and *SOD1^{G93A}* mice treated with Dafa. Endpoint was defined as the death point when mice could no longer regain their upright position within 30 s after being placed on their back, n = 10–14. (**B**) Analysis of the mean lifespan (days) of mice. (**C**) Kaplan–Meier plot of disease onset in mice. Disease onset was determined when the mice show dragging feet/knuckles. n = 6–8. (**D**) Analysis of mice disease onset (days). (**E**) Kaplan–Meier plot of paralysis in mice. Paralysis onset was defined when the mice showed single leg paralysis, n = 8–9. (**F**) Analysis of paralysis onset (days) in mice. Data are represented as mean ± SD, *p < 0.05 by one-way ANOVA.

The *ALCAT1$^{-/-}$* mice are deficient in ALCAT1 expression from embryonic day one, raising an intriguing question whether the protective effect against *SOD1^{G93A}*-induced onset of ALS could be caused by compensatory responses during embryonic development. To address this issue, we next tested the effect of Dafaglitapin (Dafa), a highly potent and selective ALCAT1 inhibitor [18], on disease progression in the *SOD1^{G93A}* mice. The male *SOD1^{G93A}* mice were orally gavaged with Dafa (10 mg/kg B.W) or vehicle (5% CM-cellulose) twice daily from the 60 days of age until death. Consistent with the findings from the *ALCAT1$^{-/-}$* mice, treatment with Dafa also prolonged the lifespan, delayed the disease onset and paralysis in the *SOD1^{G93A}* mice (Figure 1A–F).

3.2. ALCAT1 deficiency or inhibition significantly attenuates skeletal muscle atrophy and motor neuron dysfunction in the *SOD1^{G93A}* mice

ALS is characterized by denervation and skeletal muscle atrophy [3]. Accordingly, we next conducted behavioral tests, including grip

strength and rotarod tests, to determine the effect of ALCAT1 on motor neuron function in the *SOD1^{G93A}* mice. The behavioral tests were carried out in male wild type (*WT*), *SOD1^{G93A}*, and the *SOD1^{G93A}/ALCAT1$^{-/-}$* mice at the age of 120 days (Figure 2A), or *SOD1^{G93A}* mice after treatment with Dafa or vehicle by oral gavage twice daily for 60 consecutive days starting at 60 days of age (Figure 2B). The SOD1^{G93A} mutation significantly impaired neuromuscular function and coordination skills in the *SOD1^{G93A}* mice, as evidenced by decreased grip strength and running time on rotarod (Figure 2C—F). In contrast, these defects were partially attenuated by ALCAT1 deficiency (Figure 2C—D) or pharmacological inhibition by Dafa (Figure 2E—F). However, ALCAT1 deficiency or inhibition did not significantly affect the forelimb grip strength (Figure S1A-B). These findings were further supported by results from wheat germ agglutinin (WGA) staining, which showed that the SOD1 mutation caused atrophy of gastrocnemius muscle (Figure 2G—H). Consistent with improved muscle function, ablation or inhibition of ALCAT1 also partially attenuated the muscle atrophy in the hind limb of the *SOD1^{G93A}* mice, as revealed by results from hematoxylin and eosin (H&E) staining of the cross section of the gastrocnemius muscle (Figure 2G—H). Accordingly, ALCAT1 deficiency or inhibition by Dafa not only restored gastrocnemius muscle fiber size (Figure 2G—H, quantified in Figure 2I, K, and Figure S2A-B), but also muscle mass, as evidenced by the increased gastrocnemius weight to body weight ratio in the *SOD1^{G93A}* mice (Figure 2J and 2L).

3.3. Up-regulation of ALCAT1 expression by ALS is implicated in the pathogenesis of muscle atrophy and neuroinflammation

To further identify the role of ALCAT1 in the pathogenesis of ALS, we next determined the effects of ALCAT1 deficiency and inhibition on muscle morphology and mass in the quadriceps in the *SOD1^{G93A}* mice by H&E and WGA staining. Consistent with the findings in gastrocnemius, ALCAT1 deficiency or inhibition by Dafa also partially attenuated the muscle atrophy in the quadriceps of the *SOD1^{G93A}* mice, as evidenced by the increased muscle fiber size and the quadriceps weight to body weight ratio (Figure 3A—F and Figure S2C-D). To identify a causative role of ALCAT1 in the etiology of ALS, we next determine the effect of the SOD1^{G93A} mutation on ALCAT1 protein expression by western blot analysis. Strikingly, ALCAT1 protein expression was dramatically upregulated in the skeletal muscle of the *SOD1^{G93A}* mice, as evidenced by results from western blot analysis (Figure 3G, quantified in Figure 3H—I). Motor neuron deficits are associated with inflammation in the skeletal muscle of ALS patients [38]. In support of this notion, we found that the expression level of NLR Family Pyrin Domain Containing 3 (NLRP3), a key component of the NLRP3 inflammasomes, was significantly upregulated in the skeletal muscle of the *SOD1^{G93A}* mice (Figure 3G, quantified in Figure 3H—I). In addition, the mRNA expression level of several pro-inflammation cytokines, including *TNFα* and *IL-1β*, were also increased in the skeletal muscle of the *SOD1^{G93A}* mice, as revealed by results from quantitative real-time PCR (qRT-PCR) analysis (Figure 3J). Remarkably, ablation or inhibition of ALCAT1 not only attenuated the NLRP3 protein expression level, but also mRNA expression level of both *TNFα* and *IL-1β* in the skeletal muscle of the *SOD1^{G93A}* mice (Figure 3G—J), implicating a causative role of upregulated ALCAT1 expression in neuroinflammation in the *SOD1^{G93A}* mice.

3.4. Ablation or inhibition of ALCAT1 attenuates motor neurons loss and astrocyte activation in the *SOD1^{G93A}* mice

A reduction of motor neurons in the spinal cord is a major defect associated with ALS and a major cause of behavioral disorders [2]. Accordingly, we found that the *SOD1^{G93A}* mice showed progressive loss of motor neurons in the lumbar spinal cord, as evidenced by results from Nissl-stained assay (Figure 4A—B, highlighted by arrows, quantified in Figure 4C and 4E). In support of the findings from the behavioral tests, ALCAT1 deficiency and inhibition by Dafa significantly attenuated the motor neurons loss in the spinal cord of the *SOD1^{G93A}* mice (Figure 4A—B, highlighted by arrows, quantified in Figure 4C,E). A growing number of evidences suggest that neuroinflammation often leads to motor neuron degeneration both in animal models and ALS patients [39,40]. We next determined the effect of ALCAT1 on astrogliosis in the spinal cord of the *SOD1^{G93A}* mice. The results show that SOD1 mutation significantly increased the number of glial fibrillary acidic protein (GFAP) positive astrocytes, a marker of astroglial injury, in the lumbar spinal cord of the *SOD1^{G93A}* mice, as evidenced by results from immunofluorescence and immunohistochemistry analysis (Figure 4G—H, highlighted by arrows, quantified in Figure 4D,F). In contrast, ALCAT1 deficiency or inhibition by Dafa significantly decreased the number of GFAP positive astrocytes in the spinal cord of the *SOD1^{G93A}* mice (Figure 4G—H, highlighted by arrows, quantified in Figure 4D,F).

3.5. ALCAT1 deficiency or inhibition by Dafa prevents microglia activation in the *SOD1^{G93A}* mice

Microglial cells are the primary immune cells of the central nervous system. Activation of microglia promotes motor neuron death by secreting neurotoxic factors, which is implicated in the pathogenesis of ALS [41]. Accordingly, we found that the SOD1^{G93A} mutation also caused microglia activation in the spinal cord of the *SOD1^{G93A}* mice, as evidenced by results from immunofluorescent and immunohistochemical staining of ionized calcium binding adaptor molecule (IBA1), a biomarker for activated microglia (Figure 5A—B, quantified in Figure 5C—D). Consistent with the findings, the SOD1 mutation also significantly upregulated protein expression of both GFAP and IBA1 in the spinal cord of the *SOD1^{G93A}* mice, as evidenced by results from western blot analysis (Figure 5F, quantified in Figure 5G—H). Additionally, the SOD1^{G93A} mutation significantly increased mRNA expression of *TNFα* and *IL-1β*, as well as NLRP3 protein expression in the spinal cord of the *SOD1^{G93A}* mice, which was supported by results from qRT-PCR and western blot analysis (Figure 5E—F, quantified in Figure 5G—H). In further support for a causative role of upregulated ALCAT1 expression in neuroinflammation, ALCAT1 deficiency or inhibition by Dafa significantly attenuated microglia activation and downregulated the mRNA expression levels of both *TNFα* and *IL-1β* genes as well as protein expression level of NLRP3 in the spinal cord of the *SOD1^{G93A}* mice (Figure 5A—H).

3.6. ALCAT1 deficiency or inhibition prevents mitochondrial dysfunction in both spinal cord and skeletal muscle of the *SOD1^{G93A}* mice

SOD1 protein misfolding causes mitochondrial dysfunction, which is implicated in the pathogenesis of ALS through poorly defined mechanisms [42,43]. Our recent studies show that ablation of ALCAT1 prevents mitochondrial dysfunction in various age-related diseases [18,24—26,29]. We next determined the effect of ALCAT1 deficiency or inhibition by Dafa on mitochondrial ultrastructure in the skeletal muscle and spinal cord of the *SOD1^{G93A}* mice by electronic microscopy (EM) analysis. The SOD1^{G93A} mutation caused mitochondrial disarray and vacuolization in both skeletal muscle (Figure 6A, arrows highlight the enlarged mitochondria, quantified in Figure 6C) and spinal cord (Figure 6B, arrows highlight the vacuolated mitochondria, quantified in Figure 6D). In contrast, ablation of ALCAT1 or treatment with Dafa significantly restored mitochondrial morphology in both skeletal

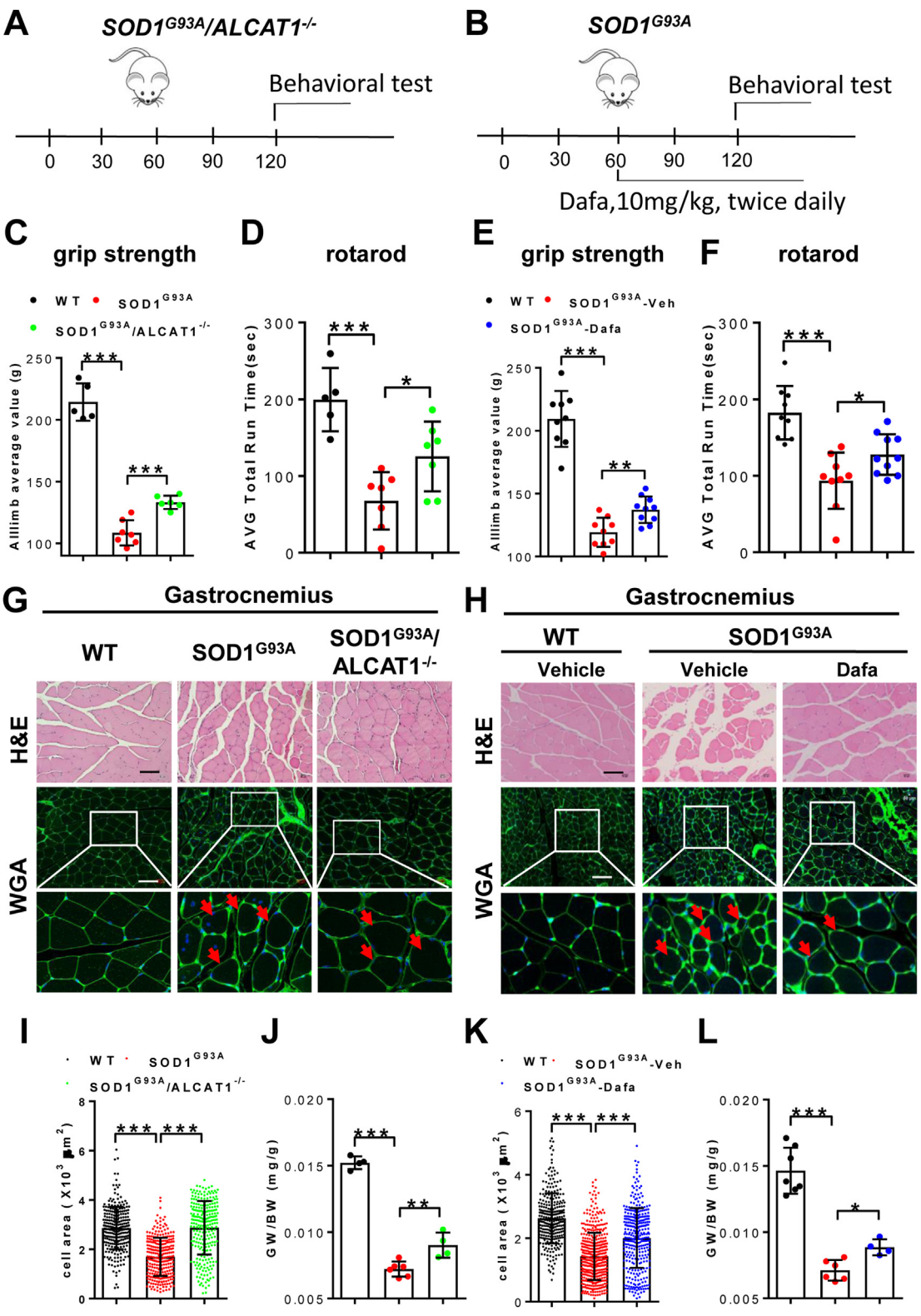

Figure 2: ALCTA1 deficiency or inhibition improves motor functions and attenuates gastrocnemius muscle atrophy in the *SOD1^{G93A}* mice. Behavioral tests of grip strength and rotarod were conducted in male mice at 4 months of age. (**A**–**B**) Diagrams depicting experimental design of behavior test in male wild-type (*WT*) control, *SOD1^{G93A}*, and *SOD1^{G93A}/ALCAT1$^{-/-}$* mice (**A**) or treatment regimen with Dafa, which were delivered by oral gavage at 10 mg/kg twice daily for 8 consecutive weeks (**B**). (**C**–**F**) Grip strength test (**C** and **E**) and rotarod test (**D** and **F**) in male mice of indicated groups at the age of 120 days. n = 5–10. (**G**–**H**) Representative images of H&E and WGA staining of the gastrocnemius muscle sections of indicated groups of mice at the age of 120 days. Arrows highlight the muscle cells. n = 3. Scale bars: 100 μm. (**I** and **K**) Quantitative analysis of muscular cell area of gastrocnemius in indicated groups of mice. 80–100 cells per mouse were used for quantification analysis. (**J** and **L**) Analysis of gastrocnemius weight to body weight ratio. n = 4–7. Data are expressed as mean ± SD, *p < 0.05, **p < 0.01, ***p < 0.001 by one-way ANOVA.

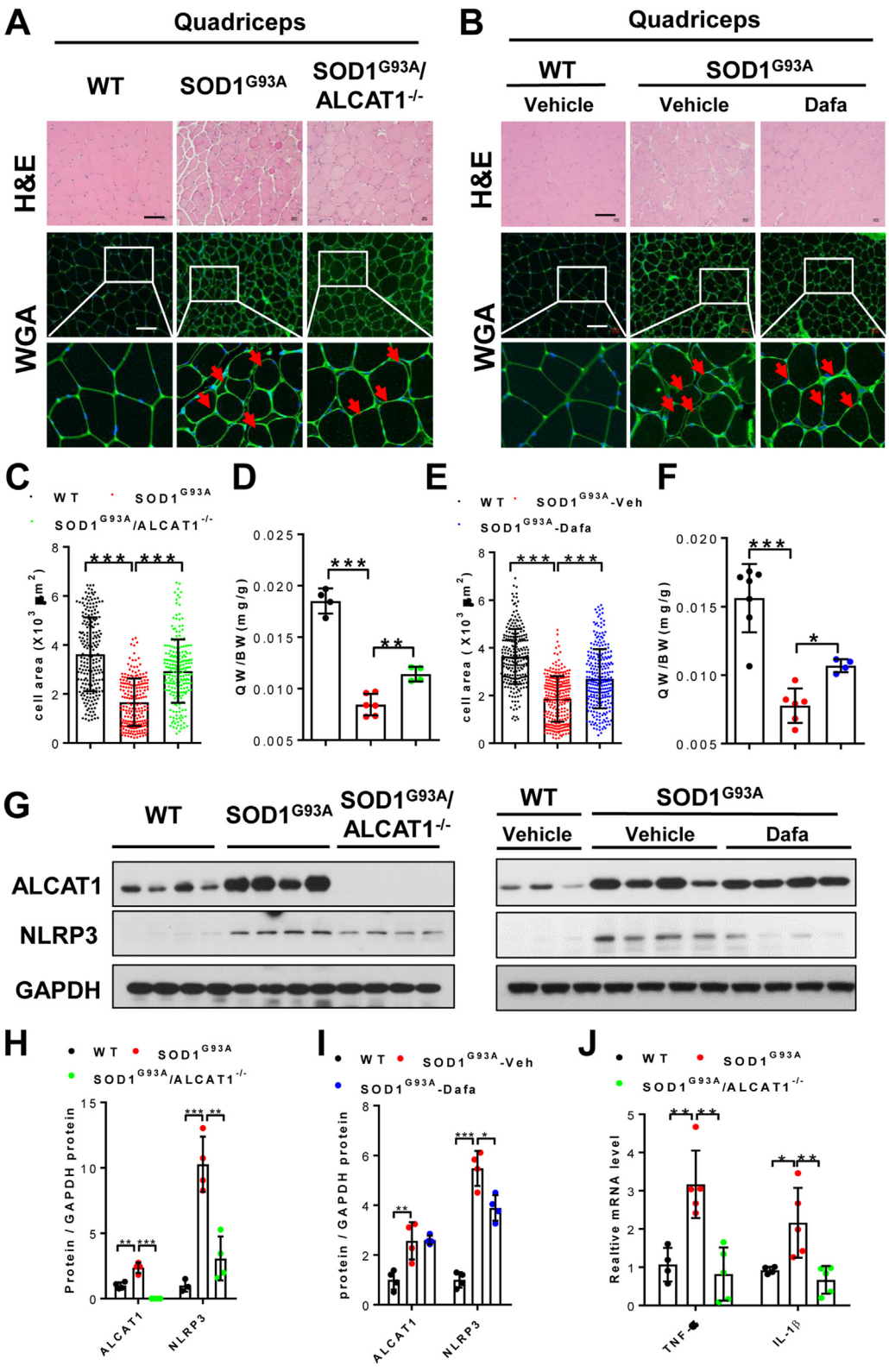

Figure 3: ALCTA1 deficiency or inhibition attenuates muscle atrophy of quadriceps femoris and inflammation in the *SOD1^{G93A}* mice. (**A**–**B**) Representative images of H&E and WGA staining of quadriceps femoris of indicated groups of mice at the age of 120 days. Arrows highlight the muscle cells. n = 3. Scale bars: 100 μm. (**C** and **E**) Quantitative analysis of individual muscular cell area of quadriceps femoris in indicated groups of mice. 70–90 cells per mouse were used for quantification analysis. (**D** and **F**) Analysis of quadriceps femoral weight to body weight ratio. n = 4–7. (**G**–**I**) Western blot analysis (**G**) and statistical analysis (**H**–**I**) of the protein expression levels of ALCAT1 and NLRP3 in mice skeletal muscle. n = 4. (**J**) qRT-PCR analysis of the mRNA levels of *TNF-α* and *IL-1β* in mice skeletal muscle. n = 4–5. Data are expressed as mean ± SD, *p < 0.05, **p < 0.01 and ***p < 0.001 by one-way ANOVA.

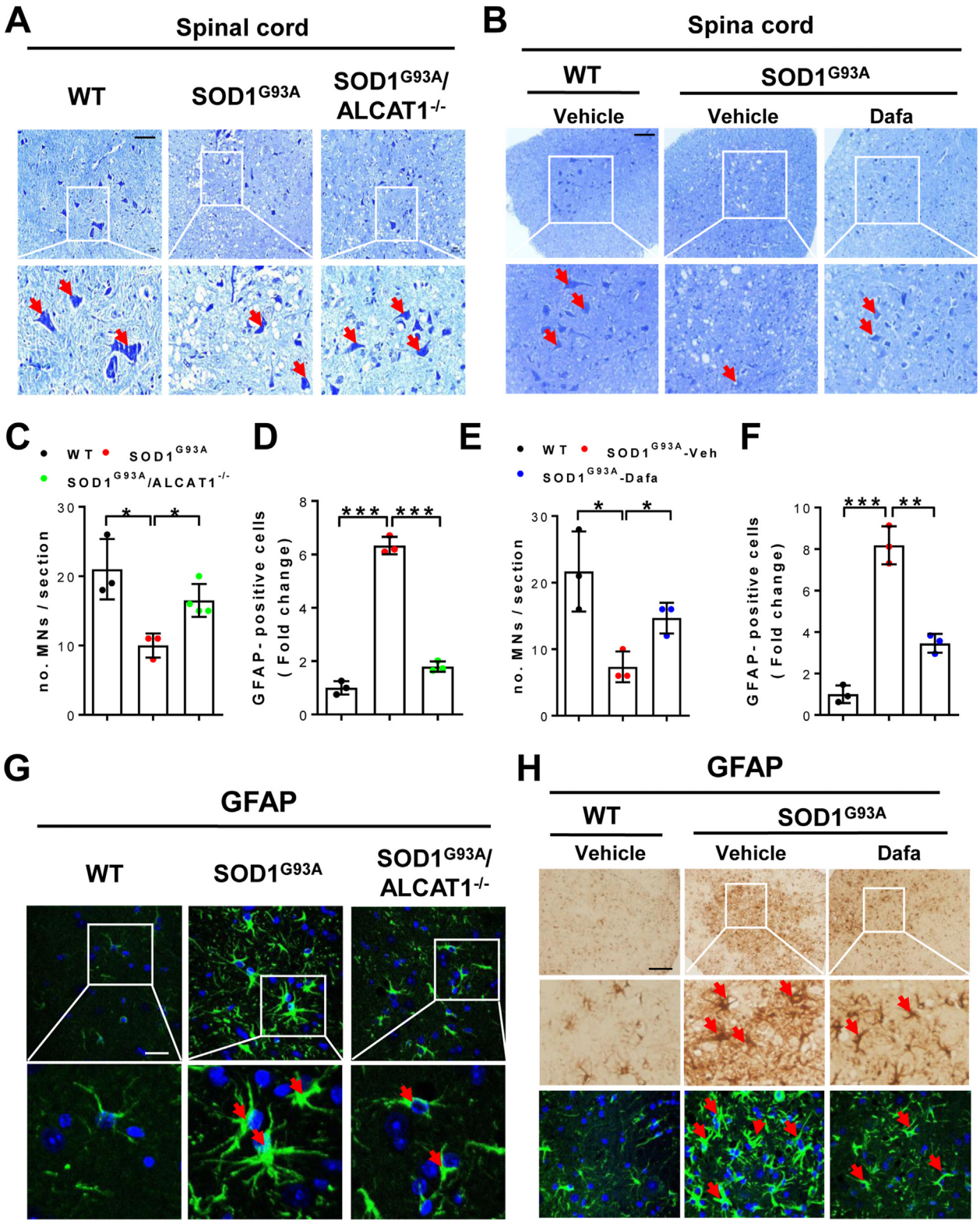

Figure 4: ALCAT1 deficiency or inhibition mitigates motor neuron loss and astrocytes activation in the lumbar spinal cord of the *SOD1^{G93A}* mice. (**A**–**B**) Representative images of Nissl stained in the lumbar spinal cord of indicated groups of mice at the age of 120 days. Arrows highlighted the motor neurons. Scale bars: 200 μm. (**C** and **E**) Quantitative analysis of the number of motor neurons in mice lumbar spinal cord. n = 3. (**D** and **F**) Quantitative analysis of GFAP-positive astrocytes in mice lumbar spinal corde. n = 3. (**G**) Immunofluorescent imaging analysis of GFAP-positive astrocytes in the lumbar spinal cord of indicated groups of mice at the age of 120 days. Tissue samples were immunoblotted with anti-GFAP (green) and DAPI (blue) for nucleus staining, followed by confocal imaging analysis of GFAP-positive astrocytes, highlighted by arrows. Scale bars: 20 μm. (**H**) Immunohistochemical and immunofluorescent imaging analysis of GFAP-positive astrocytes in the lumbar spinal cord sections of *WT* control and *SOD1^{G93A}* mice treated with Dafa or vehicle. Arrows highlight the GFAP-positive astrocytes. Scale bar: 200 μm. Data are expressed as mean ± SD, *p < 0.05, ***p < 0.001 by one-way ANOVA.

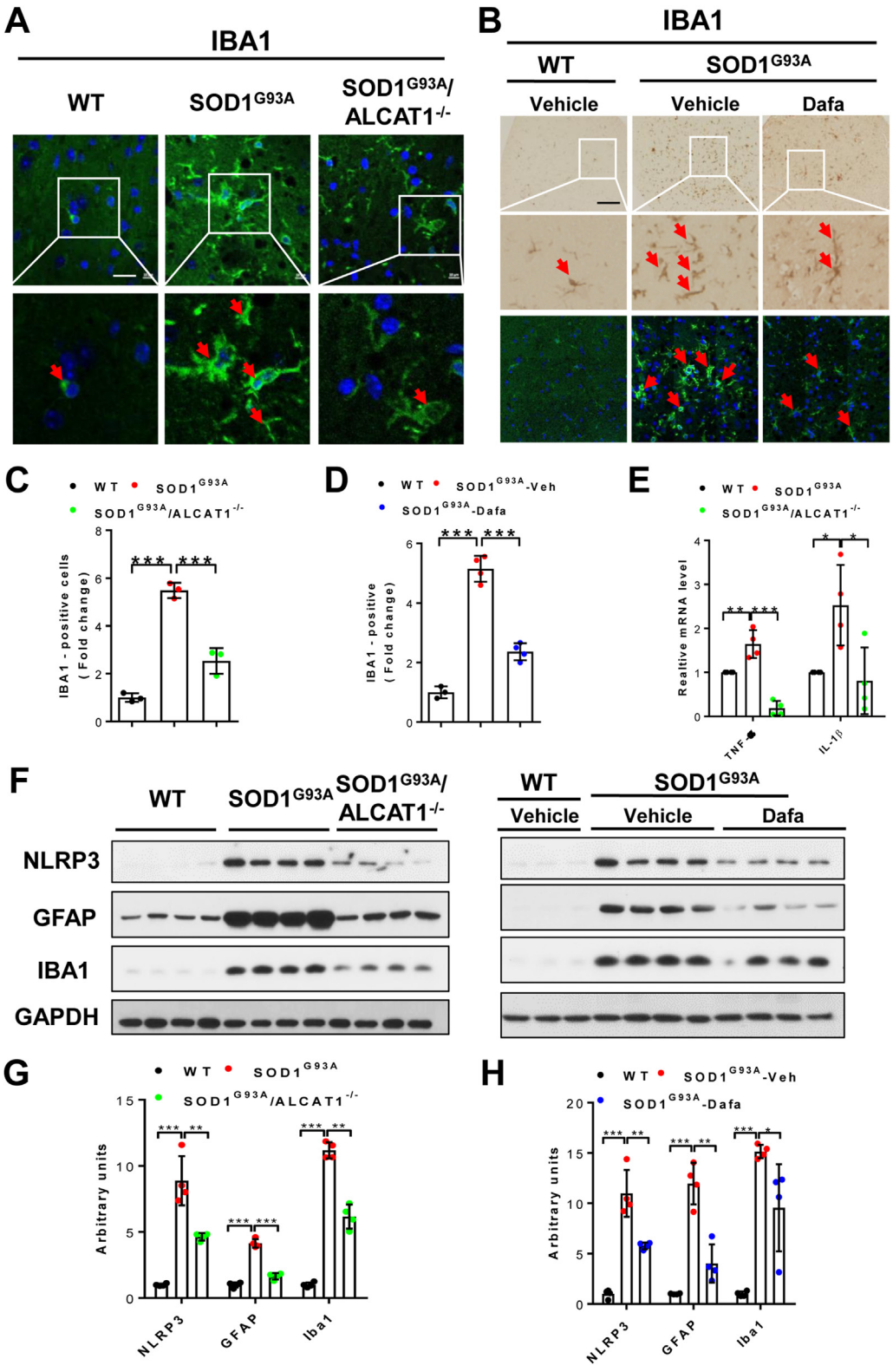

Figure 5: Ablation or inhibition ALCAT1 by Dafa mitigates microglial activation and inflammation in the lumbar spinal cord of the *SOD1^{G93A}* mice. (**A**) Immunofluorescent imaging analysis of IBA1-positive microglia in the lumbar spinal cord sections of indicated groups of mice at the age of 120 days. Tissue samples were immunoblotted with anti-IBA1 (green) and DAPI (blue) for nucleus staining, followed by confocal imaging analysis of IBA1-positive microglia, highlight by arrows. Scale bars: 20 μm (**B**) Immunohistochemical and immunofluorescent imaging analysis of IBA1-positive microglia in the lumbar spinal cord sections of *WT* control and *SOD1^{G93A}* mice treated with Dafa or vehicle. Arrows highlight the IBA1-positive microglia. Scale bars: 200 μm. (**C**—**D**) Quantitative analysis of IBA1-positive microglia in mice lumbar spinal cord. n = 3. (**E**) qRT-PCR analysis of the mRNA levels of *TNF-α* and *IL-1β* in the spinal cord of *WT* control, *SOD1^{G93A}*, and *SOD1^{G93A}/ALCAT1$^{-/-}$* mice at the age of 120 days. n = 4. (**F**—**H**) Western blot analysis (**F**) and statistical analysis (**G**—**H**) of the expression levels of NLRP3, GFAP, and IBA1 in mice spinal cord. n = 4. Data are expressed as mean ± SD, *p < 0.05, **p < 0.01, ***p < 0.001 by one-way ANOVA.

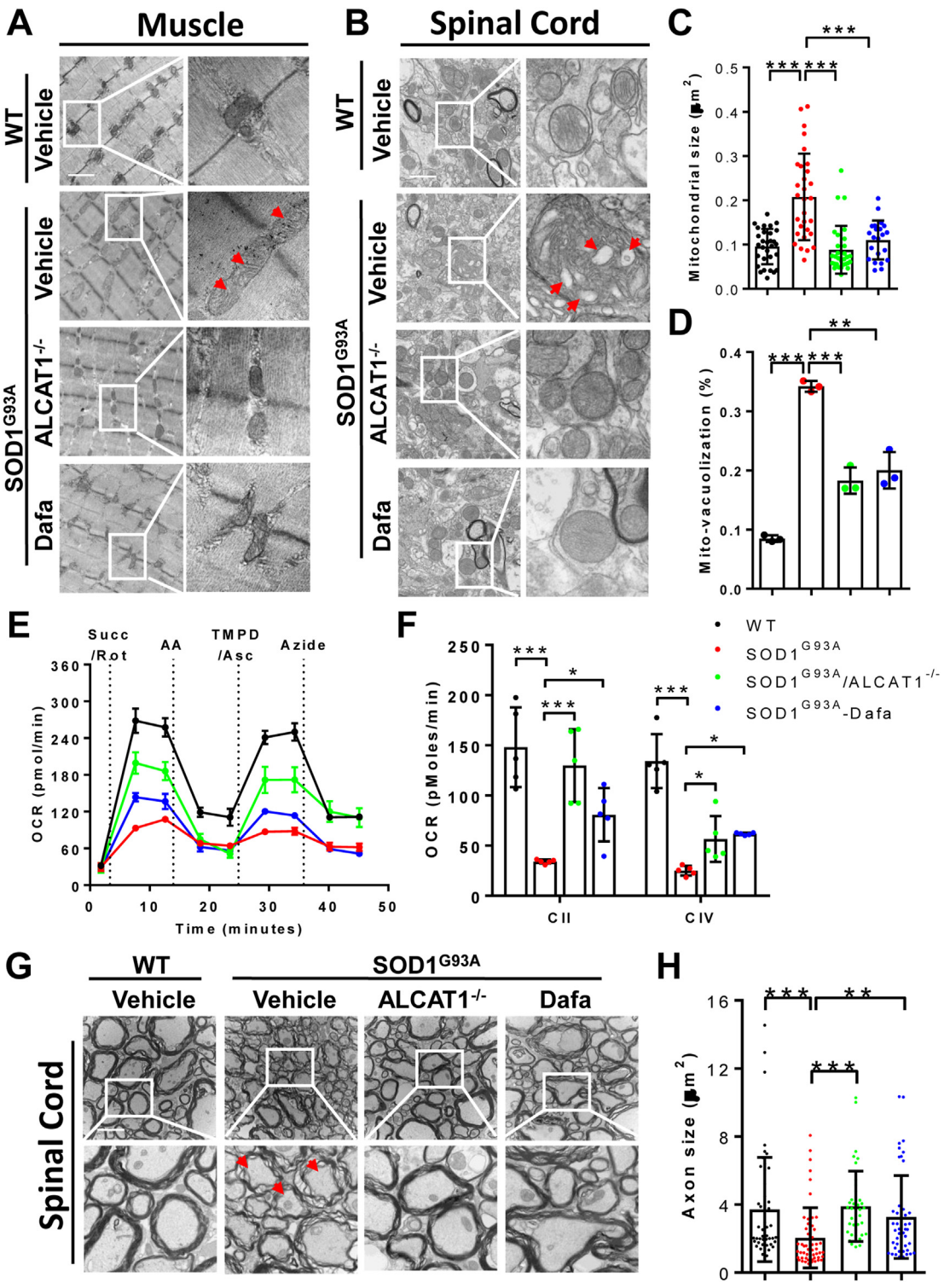

Figure 6: Ablation or inhibition ALCAT1 mitigates mitochondrial dysfunction in the muscle and spinal cord of the *SOD1^{G93A}* mice. (**A**–**B**) EM analysis of mitochondrial morphology and organization in mice skeletal muscle (**A**) and spinal cord (**B**). Arrows highlight the swollen mitochondria. Scale bar: 1.2 μm. (**C**) Quantitative analysis of mitochondrial size in mice skeletal muscle. (**D**) Quantitative analysis of vacuolated mitochondria in mice spinal cord. n = 3, and 50 mitochondria per mouse were counted. (**E**) Seahorse analysis of OCR in mitochondria isolated from frozen spinal cord samples in response to succinate/rotenone (Succ/Rot), antimycin A (AA), TMPD/ascorbate (TPMD/Asc), and sodium azide treatment. n = 5. (**F**) Quantitative analysis of Succ/Rot (complex II)- and TMPD/Asc (complex IV, CIV)-dependent respiration in panel **E**. (**G**) EM analysis of axon morphology in mice spinal cord. Scale bar: 2 μm. Arrows highlight the damaged myelin sheets. (**H**) Quantitative analysis the axon size in mice spinal cord. Data are expressed as mean ± SD, $^{**}p < 0.01$, $^{***}p < 0.001$ by one-way ANOVA.

muscle and spinal cord of the *SOD1^{G93A}* mice (Figure 6A-D). We next determined the mitochondrial respiration in isolated mitochondria from frozen spinal cord samples, followed by analysis for mitochondrial respiration by Seahorse flux analyzer according to the protocol as previously described [23,35]. The results showed that the SOD1^{G93A} mutation significantly decreased mitochondrial OCR in response to treatments with the succinate/rotenone (complex II respiration) and TMPD/ascorbate (complex IV respiration) in isolated mitochondria from the spinal cord of the SOD1^{G93A} mice (Figure 6E, quantified in Figure 6F). Consistent with normalization in mitochondrial morphology, ALCAT1 deficiency or inhibition by Dafa also partially restored the mitochondrial complex II and complex IV respiration in the spinal cord mitochondria of the SOD1^{G93A} mice (Figure 6E—F). Additionally, the SOD1^{G93A} mutation also significantly decreased axon size and damaged myelin sheets in the spinal cord of the *SOD1^{G93A}* mice (Figure 6G, highlighted by arrows, and quantified in Figure 6H). Again, these defects were mitigated by either ALCAT1 deficiency or inhibition by Dafa, as evidenced by results from EM analysis of axon morphology of the spinal cord (Figure 6G—H).

3.7. ALCAT1 links oxidative stress to SOD1 protein aggregation in the *SOD1^{G93A}* mice

The presence of the SOD1 oligomers is a major defect in ALS, as reported by previous studies [44,45]. To gain further insights on mechanisms by which upregulated ALCAT1 expression promotes the development of ALS, we next investigated gain and loss of ALCAT1 function in regulating the SOD1^{G93A} protein aggregation in the *SOD1^{G93A}* mice and in NSC-34 cell line, a mouse motor neuron-like hybrid cell line. In agreement with the previous report [46], the SOD1^{G93A} mutation caused severe aggregation of the SOD1 protein in the spinal cord of the *SOD1^{G93A}* mice, as evidenced by presence of high molecular weight oligomers of the SOD1^{G93A} mutant protein when resolved by non-reducing PAGE analysis (Figure 7A). In contrast, ALCAT1 deficiency significantly attenuated the oligomerization of the mutant SOD1 protein in the spinal cord of the *SOD1^{G93A}* mice (Figure 7A). To further confirm the findings, we next generated a NSC-34 stable cell line with targeted deletion of ALCAT1 by using *CRISPR/Cas9*-mediated gene editing technology. The stable NSC-34 cell line is completely deficient in ALCAT1 protein expression, as confirmed by results from western blot analysis (Figure 7B). In contrast to the WT SOD1 protein, the SOD1^{G93A} mutant protein aggregated when transiently expressed in NSC-34 vector control cells (Figure 7C). In further support of a causative role of upregulated ALCAT1 protein expression in the pathogenesis of ALS, ALCAT1 deficiency significantly attenuated SOD1^{G93A} mutant protein aggregation, whereas adenoviral overexpression of ALCAT1 significantly exacerbated aggregation of the SOD1^{G93A} mutant protein in NSC-34 cells (Figure 7C—D).

Oxidative stress is implicated in the aggregation of the SOD1 mutant protein, yet the underlying causes of oxidative stress by ALS remain poorly understood [47]. Our previous work showed that upregulated ALCAT1 expression by ROS links oxidative stress to mitochondrial dysfunction in age-related metabolic diseases by promoting CL peroxidation [24,25]. To determine whether ALCAT1 promotes the SOD1 protein aggregation through oxidative stress, we next measured the ROS level in NSC-34 cells transiently expressed either the WT SOD1 or the SOD1^{G93A} mutant. As shown by Figure 7E, overexpression of the SOD1^{G93A} in NSC-34 cells significantly increased ROS production, which was further exacerbated by treatment with hydrogen peroxide (H_2O_2) (Figure 7E). In agreement with previous study [47], H_2O_2 treatment also induced the SOD1^{G93A} protein aggregation in NSC-34 cells (Figure 7F). Strikingly, ALCAT1 deficiency or inhibition by Dafa significantly attenuated H_2O_2-induced ROS production in NSC-34 neuronal cells overexpressing the SOD1^{G93A} mutant (Figure 7E). Consistently, treatment with Dafa also dose-dependently attenuated H_2O_2-induced SOD1^{G93A} protein aggregation in NSC-34 cells (Figure 7F).

3.8. ALCAT1 deficiency or inhibition by Dafa restores CL content and acyl compositions in the spinal cord of *SOD1^{G93A}* mice

As the mitochondrial signature phospholipid, CL plays a crucial role in maintaining normal metabolic function in the brain, as highlighted by the increasing number of neurodegenerative diseases linked with CL abnormalities, including PD and AD [29,48,49]. In contrast to metabolic tissues, both linoleic acid and DHA are major constituents of CL in the brain [50], which likely renders CL even more sensitive to damage by ROS associated with aging than metabolic tissues. However, surprisingly little information is known as to how CL is remodeled in the spinal cord during the onset of ALS. Our previous work showed that ALCAT1 catalyzes the pathological remodeling of CL with DHA and other polyunsaturated fatty acids in metabolic tissues, leading to oxidative stress and mitochondrial dysfunction [18,24,26,29]. We next determined the effects of SOD1^{G93A} mutation and ALCAT1 deficiency on CL contents and acyl compositions in the spinal cord of the SOD1^{G93A} mice by lipidomic analysis using protocol as previously reported [24]. The results showed that SOD1^{G93A} mutation significantly reduced the levels of total CL and CL species enriched with DHA (22:6) and arachidonic acid (AA) (20:4) in mice spinal cord (Figure 8A—C). Consistent with improved mitochondrial morphology and function, ALCAT1 deficiency or inhibition by Dafa not only restored total CL content, but also the levels of CL species enriched with DHA and AA in the spinal cord of SOD1^{G93A} mice (Figure 8A—C). Additionally, ALCAT1 deficiency or inhibition by Dafa also restored the levels of other CL species which were significantly reduced in the spinal cord of SOD1^{G93A} mice (Figure 8D—E). Our findings are corroborated by a previous report that the SOD1^{G93A} mutation significantly reduced CL content and CL species enriched with DHA and AA [30], implicating an important role of CL species enriched with DHA and AA in supporting the normal mitochondrial function of the spinal cord.

4. DISCUSSION

ALS is a fatal neurodegenerative disease characterized by selective death of motor neurons. There are no effective treatments for ALS, since the underlying causes of this deadly disorder are largely unknown. Mutations in SOD1 are the major culprit of familial ALS and abnormal SOD1 aggregation in the motor neurons have been suggested as the major pathological hallmark of ALS [51—53]. However, the underlying causes of SOD1 protein aggregation in ALS remain elusive. In this study, we identified ALCAT1 as a key mediator of SOD1 protein aggregation and ALS progression. We show that SOD1^{G93A} mutation caused accumulation of SOD1 protein aggregations in the spinal cord of the *SOD1^{G93A}* transgenic mice, leading to skeletal muscle atrophy, neuronal inflammation, motor neurons loss and mitochondrial dysfunction. These defects were moderately mitigated by targeted deletion of the *ALCAT1* gene or pharmacological inhibition of ALCAT1 enzyme by Dafa. Consequently, ablation or pharmacological inhibition of ALCAT1 by Dafa not only mitigated mitochondrial dysfunction, but also attenuated motor neurons loss, skeletal muscle atrophy, and neuroinflammation, leading to delay in disease onset, improvement in motor function, and extension of lifespan of the *SOD1^{G93A}* mice. Consistent with the findings, ALCAT1 deficiency or

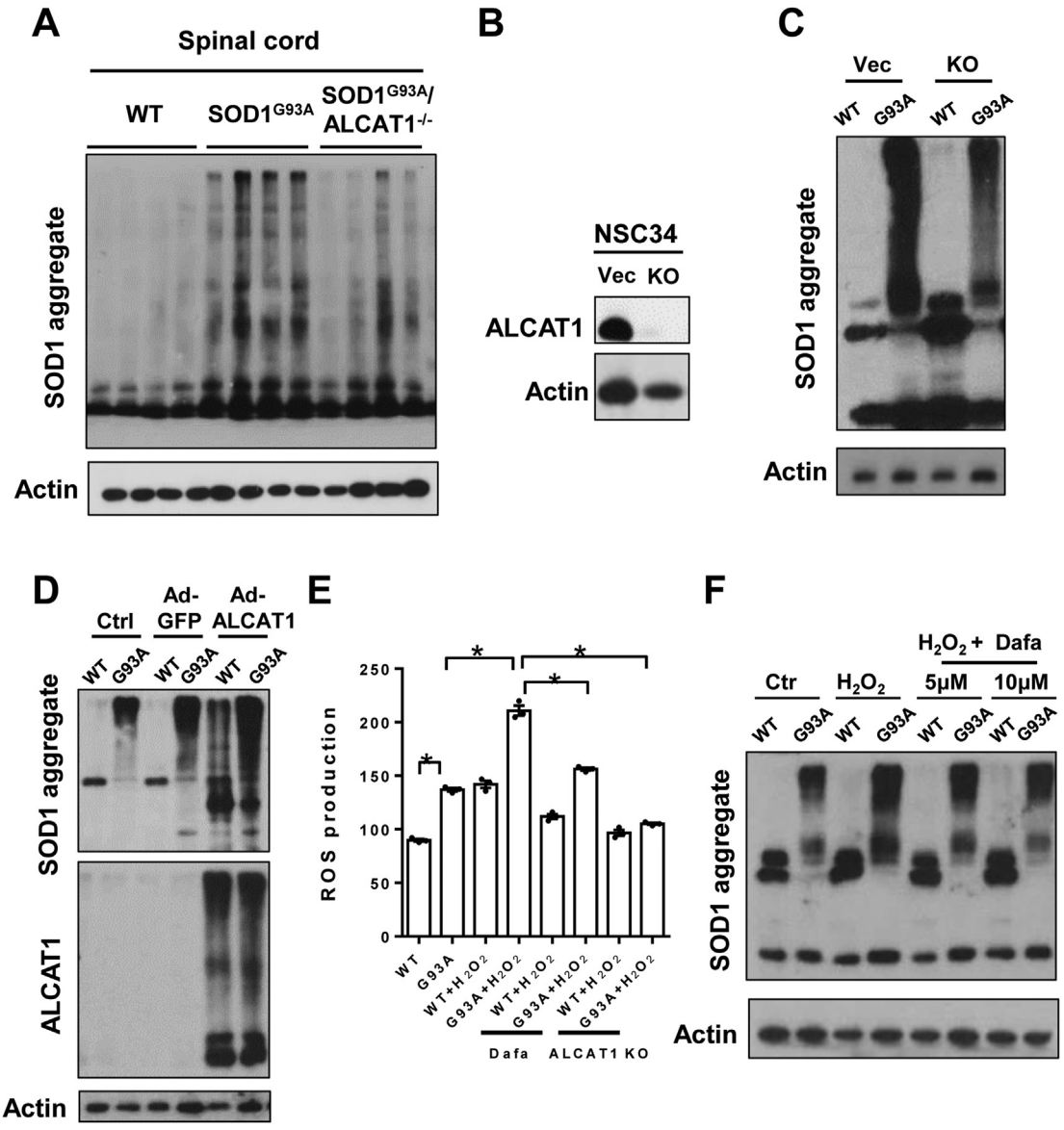

Figure 7: ALCAT1 promotes SOD1 protein aggregation in mice spinal cord and NSC-34 cells through oxidative stress. (**A**) Western blot analysis of the SOD1 aggregates in the spinal cord of indicated groups of mice at the age of 120 days. Insoluble fractions of spinal cord tissues lysates were resuspended in non-denaturing loading buffer, and immunoblotted with anti-SOD1 antibody. (**B**) Western blot analysis of ALCAT1 protein expression in NSC-34 vector control and ALCAT1 deficient cells. (**C**) Western blot analysis of the SOD1 protein aggregates in vector control and ALCAT1 deficient NSC-34 cells. The cells were transiently transfected with either WT GFP-SOD1 or GFP-SOD1^{G93A}. The insoluble fractions of the cell lysates were immunoblotted with an anti-SOD1 antibody, and soluble fractions were immunoblotted with anti-β-actin antibody. (**D**) Western blot analysis of the SOD1 protein aggregates in vector control and ALCAT1 overexpression NSC-34 cells. NSC-34 cells were transiently transfected with either WT GFP-SOD1 or GFP-SOD1^{G93A} for 24 h, followed by infection with Ad-GFP virus or Ad-ALCAT1 virus for another 24 h. The insoluble fractions of the cell lysates were immunoblotted with an anti-SOD1 antibody, and soluble fractions were immunoblotted with anti-ALCAT1 and anti-β-actin antibodies. (**E**) Measurement of intracellular ROS level in NSC-34 cells. The cells transiently expressed either WT GFP-SOD1 or GFP-SOD1^{G93A} were pretreated with Dafa (10 μM) or vehicle for 2 h, followed by H_2O_2 (200 μM) treatment in the presence or absence of Dafa for 3 h. The intracellular ROS was determined by using H_2DCFDA. n = 3. (**F**) Western blot analysis of the SOD1 protein aggregates in NSC-34 cells in response to Dafa and H_2O_2 treatment. The cells transiently expressed either WT GFP-SOD1 (WT) or GFP-SOD1^{G93A} were pretreated with Dafa (10 μM) or vehicle for 2 h, followed by H_2O_2 (200 μM) treatment in the presence or absence of Dafa for 3 h. The insoluble fractions of the cell lysates were immunoblotted with an anti-SOD1 antibody, and soluble fractions were immunoblotted with anti-β-actin antibody. Data are expressed as mean ± SD, *p < 0.05 by two-way ANOVA.

inhibition also restored CL content and acyl compositions in the spinal cord of *SOD1^{G93A}* mice.

Protein aggregation has been a common pathological feature of neurodegenerative diseases, including β-amyloid and tau tangles in Alzheimer's disease as well as α-synuclein protein aggregation in PD, huntingtin in Huntington's disease, and SOD1 aggregation in ALS [54,55]. The formation of the SOD1-positive inclusions in familial ALS patients and animal models supports SOD1 aggregation as the underlying cause of familial ALS [56]. Accumulation of SOD1 aggregation also caused damage to mitochondrial morphology and function, such as leakage of the outer mitochondrial membrane and expansion of the intermembrane space, leading to mitochondrial swelling and vacuolization, loss of oxidative phosphorylation capacity, and reduction in ATP synthesis in motor neurons, all of which have been implicated in early

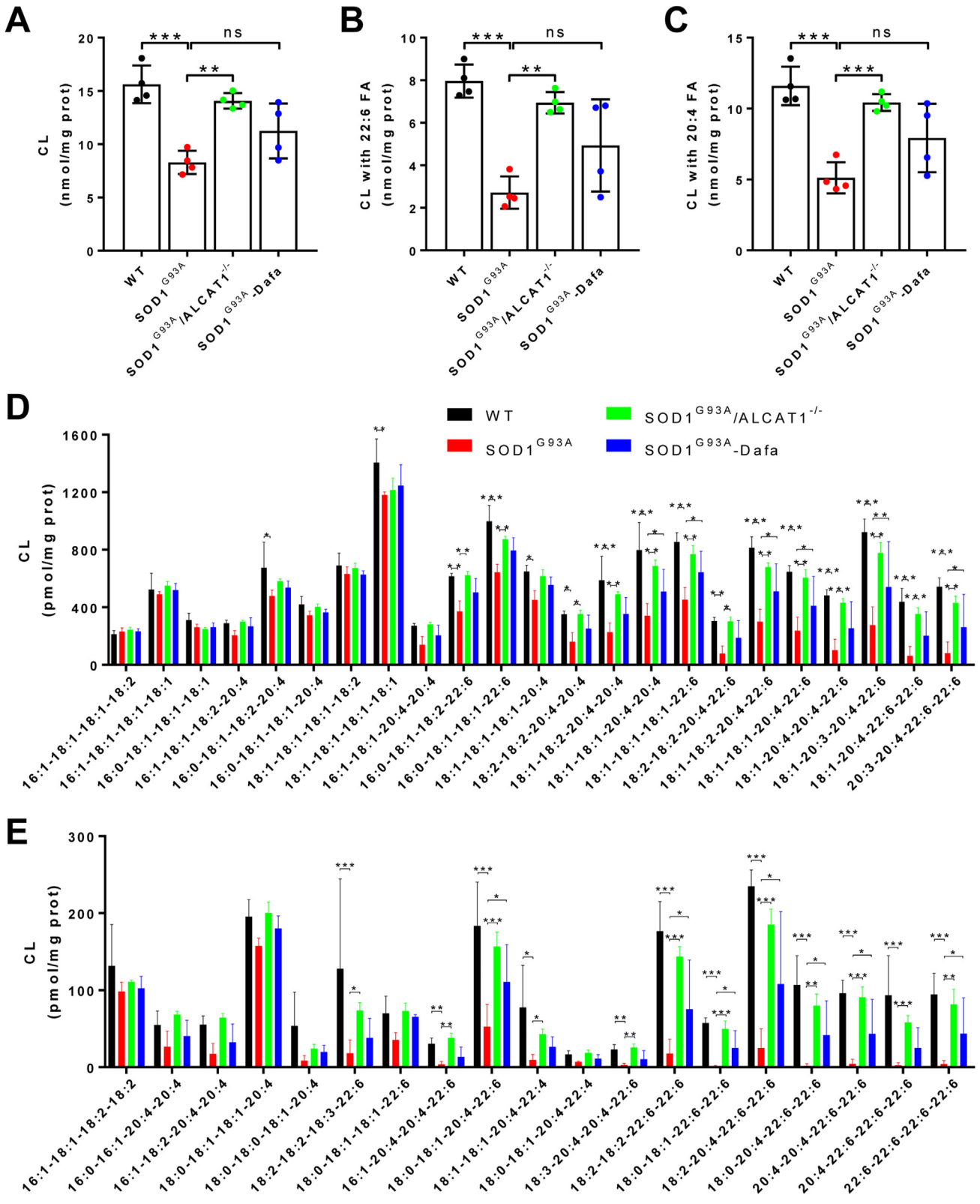

Figure 8: Ablation or inhibition of ALCAT1 restores CL level and acyl compositions in the spinal cord of *SOD1^{G93A}* mice. Lipids extracted from mice spinal cord at the age of 120 days were used for lipidomic analysis CL levels and acyl compositions by ESI/MS. (**A**–**C**) The levels of total CL (**A**) and CL enriched with DHA (22:6, **B**) or arachidonic acid (20:4, **C**) in mice spinal cord. (**D**–**E**) Lipidomics profiling of all major CL species in the spinal cord of indicated groups of mice. n = 4. Data are expressed as mean ± SD, $^{**}p < 0.01$, $^{***}p < 0.001$ by one-way ANOVA. ns, no significance.

pathological features of familial ALS in rodent models and patients [9,42,57]. The SOD1^{G93A} mutation not only causes destabilization, misfolding, and aggregation of SOD1, but also leads to oxidative stress and CL peroxidation, resulting in a vicious circle that further exacerbates the pathogenesis of ALS [31,47,58,59]. In this study, we identified a critical role of ALCAT1 in regulating SOD1 aggregation through oxidative stress, linking mitochondrial dysfunction to ALS in the *SOD1^{G93A}* mice. In support of this notion, we showed that ALCAT1 expression is upregulated by ALS, and overexpression of ALCAT1 exacerbated the SOD1^{G93A} protein aggregation in both spinal cord and NSC-34 neuronal cell line. Consequently, ALCAT1 deficiency or inhibition significantly attenuated the SOD1^{G93A} protein aggregation in the spinal cord of the *SOD1^{G93A}* mice and in NSC-34 neuronal cell line. In support a key role of ALCAT1 in promoting oxidative stress by ALS, inhibition of ALCAT1 by Dafa not only attenuated the SOD1^{G93A}-induced oxidative stress, but also mitigated H_2O_2-inducd SOD1^{G93A} aggregation in NSC-34 neuronal cells. These findings are consistent with our previous report that upregulated ALCAT1 expression by ROS caused severe oxidative stress [24], leading to mitochondrial dysfunction and the development of various age-related diseases [18,24–26,29]. Additionally, ablation or pharmacological inhibition of ALCAT1 also significantly attenuated protein aggregation of α-synuclein in a mouse model of PD [29]. Our findings are also corroborated by previous reports that oxidative stress contributed to the aggregation of SOD1, and inhibition of oxidative stress attenuated SOD1 aggregation and ALS progression [47,59]. Furthermore, Edaravone, one of the only two drugs approved for ALS by FDA, attenuates neuronal dysfunction as a strong antioxidant.

ALS pathology is intimately linked with neuroinflammation, specifically activation and recruitment of microglia and astrocytes, which contributes to the loss of motor neurons [60]. However, the molecular mechanisms underlying the causes of gliosis and neuroinflammation remain largely unknown. Extracellular SOD1^{G93A} mutant protein has been shown to stimulate the expression of pro-inflammatory cytokines, such as *TNF-α*, *IL-1β*, in primary microglia and microglial BV2 cells, leading to activation of microglia [61,62]. Additionally, accumulation of the SOD1 aggregates in the spinal motor neurons and glia cells lead to the activation of microglia through the lipid raft, providing a potential link between protein aggregation and gliosis in ALS [63]. Accordingly, ablation of the mutant SOD1 in either astrocytes or microglia moderately slowed disease progression and extended lifespan in ALS mice, which suggested that motor neurons degeneration can result from a non-cell autonomous effect of the mutant SOD1 [64,65]. In agreement with previous findings, we showed in this study that the SOD1^{G93A} mutation caused activation of astrocytes and microglia, leading to neuronal inflammation and motor neurons loss in the spinal cord of the *SOD1^{G93A}* mice. In contrast, ALCAT1 deficiency or inhibition by Dafa mitigated the activation of astrocytes and microglia as well as motor neurons loss in the spinal cord of the *SOD1^{G93A}* mice. Moreover, we showed that ALCAT1 deficiency or inhibition also significantly attenuated NLRP3 inflammasome activation in the spinal cord of the *SOD1^{G93A}* mice, which is consistent with a previous report that NLRP3 inflammasome activation contributes to the pathogenesis of chronic inflammatory and neuronal apoptosis in ALS [66].

Despite intensive efforts by pharmaceutical industries in recent years, there are no effective treatments for ALS. To date, Riluzole and Edaravone are the only two drugs approved by FDA for the treatment of ALS patients [67]. However, neither drug is highly effective in treating this lethal condition. Riluzole, a glutamatergic neurotransmission inhibitor, moderately delayed the initiation of respiratory dysfunction and extended the median survival of patients for 2–3 months [6]. Yet, Riluzole failed to attenuate motor dysfunction and did not benefit older and more severe patients [68]. Edaravone is an antioxidant drug which has been shown to moderately slow disease progression in ALS patients [5]. However, the precise molecular mechanisms of Riluzole and Edaravone remains to be fully understood, and neither of the treatment targets the root cause of ALS, which explains their poor efficacy in treating ALS. Therefore, it remains a major challenging and urgent task to develop more effective treatments for ALS. Toward this end, our findings have provided key insights on targeting ALCAT1 as a potential strategy to treat ALS from the following perspectives. First, upregulation of ALCAT1 plays a causative role in the pathogenesis of ALS, linking SOD1 aggregation to mitochondrial etiology of this disease. Second, the ALCAT1 enzyme is completely druggable, as demonstrated by this study that Dafa, a very potent and highly selective small molecule inhibitor of ALCAT1, successfully delayed the onset of ALS disease and extended the lifespan of the *SOD1^{G93A}* mice. Third, ALCAT1 inhibitor may provide additional benefits to ALS patients, since up-regulated ALCAT1 protein expression is also implicated in the pathogenesis of age-related diseases, including obesity, type 2 diabetes, non-alcohol fatty liver disease, cardiovascular diseases, and PD [18,24–26,29]. Taken together, our data has provided key insights on targeting the ALCAT1 enzyme as a potential treatment of ALS with completely different mechanisms of action for this lethal disorder.

AUTHOR CONTRIBUTIONS

Y.S. conceived the project and designed the research plan. X.L. J.Z., J.L. and C.S. performed the experiments. X.L., and J.Z. analyzed the data. Y.S., J.Z., and X.L. wrote the manuscript and all authors edited it.

DATA AVAILABILITY STATEMENT

The data that support the findings of this study are available from the corresponding author upon reasonable request.

ACKNOWLEDGEMENTS

We would like to thank Dr. Xianlin Han for technical assistance on lipidomic analysis and Dr. John-Paul Andersen for critically reading this manuscript. This work was supported in part by funding from the NIH (R01AG055747, Y.S., P30AG013319, Y.S.), American Diabetes Association (#1-18 IBS-329, Y.S.), Barth Syndrome Foundation (Y.S. and J.Z.), William and Ella Owens Medical Research Foundation (Y.S. and J.Z.), and an endowment from Joe R. and Teresa Lozano Long Distinguished Chair in Metabolic Biology (Y.S.).

CONFLICT OF INTEREST

Y.S. is a shareholder of Perenna Pharmaceuticals Inc, a privately held company which provided the ALCAT1 inhibitor Dafa used in this study. The other authors declare no competing interests.

APPENDIX A. SUPPLEMENTARY DATA

Supplementary data to this article can be found online at https://doi.org/10.1016/j.molmet.2022.101536.

REFERENCES

[1] Shang, H., Liu, G., Jiang, Y., Fu, J., Zhang, B., Song, R., et al., 2015. Pathway analysis of two amyotrophic lateral sclerosis GWAS highlights shared genetic

signals with Alzheimer's disease and Parkinson's disease. Molecular Neurobiology 51(1):361—369.
[2] Walling, A.D., 1999. Amyotrophic lateral sclerosis: Lou Gehrig's disease. American Family Physician 59(6):1489—1496.
[3] Kiernan, M.C., Vucic, S., Cheah, B.C., Turner, M.R., Eisen, A., Hardiman, O., et al., 2011. Amyotrophic lateral sclerosis. Lancet 377(9769):942—955.
[4] Wijesekera, L.C., Leigh, P.N., 2009. Amyotrophic lateral sclerosis. Orphanet Journal of Rare Diseases 4:3.
[5] Abe, K., Aoki, M., Tsuji, S., Itoyama, Y., Sobue, G., Togo, M., et al., 2017. Safety and efficacy of edaravone in well defined patients with amyotrophic lateral sclerosis: a randomised, double-blind, placebo-controlled trial. The Lancet Neurology 16(7):505—512.
[6] Bensimon, G., Lacomblez, L., Meininger, V., 1994. A controlled trial of riluzole in amyotrophic lateral sclerosis. ALS/Riluzole Study Group. New England Journal of Medicine 330(9):585—591.
[7] Rosen, D.R., Siddique, T., Patterson, D., Figlewicz, D.A., Sapp, P., Hentati, A., et al., 1993. Mutations in Cu/Zn superoxide dismutase gene are associated with familial amyotrophic lateral sclerosis. Nature 362(6415):59—62.
[8] Valentine, J.S., Doucette, P.A., Zittin Potter, S., 2005. Copper-zinc superoxide dismutase and amyotrophic lateral sclerosis. Annual Review of Biochemistry 74:563—593.
[9] Higgins, C.M., Jung, C., Xu, Z., 2003. ALS-associated mutant SOD1G93A causes mitochondrial vacuolation by expansion of the intermembrane space and by involvement of SOD1 aggregation and peroxisomes. BMC Neuroscience 4:16.
[10] Kong, J., Xu, Z., 1998. Massive mitochondrial degeneration in motor neurons triggers the onset of amyotrophic lateral sclerosis in mice expressing a mutant SOD1. Journal of Neuroscience 18(9):3241—3250.
[11] Claypool, S.M., Koehler, C.M., 2012. The complexity of cardiolipin in health and disease. Trends in biochemical sciences 37(1):32—41.
[12] Hatch, G.M., 2004. Cell biology of cardiac mitochondrial phospholipids. Biochemistry and Cell Biology 82(1):99—112.
[13] Paradies, G., Paradies, V., De Benedictis, V., Ruggiero, F.M., Petrosillo, G., 2014. Functional role of cardiolipin in mitochondrial bioenergetics. Biochimica et Biophysica Acta 1837(4):408—417.
[14] Schlame, M., Rua, D., Greenberg, M.L., 2000. The biosynthesis and functional role of cardiolipin. Progress in Lipid Research 39(3):257—288.
[15] Shi, Y., 2010. Emerging roles of cardiolipin remodeling in mitochondrial dysfunction associated with diabetes, obesity, and cardiovascular diseases. J Biomed Res 24(1):6—15.
[16] Han, X., Yang, J., Cheng, H., Yang, K., Abendschein, D.R., Gross, R.W., 2005. Shotgun lipidomics identifies cardiolipin depletion in diabetic myocardium linking altered substrate utilization with mitochondrial dysfunction. Biochemistry 44(50):16684—16694.
[17] Han, X., Yang, J., Yang, K., Zhao, Z., Abendschein, D.R., Gross, R.W., 2007. Alterations in myocardial cardiolipin content and composition occur at the very earliest stages of diabetes: a shotgun lipidomics study. Biochemistry 46(21):6417—6428.
[18] Jia, D., Zhang, J., Nie, J., Andersen, J.P., Rendon, S., Zheng, Y., et al., 2021. Cardiolipin remodeling by ALCAT1 links hypoxia to coronary artery disease by promoting mitochondrial dysfunction. Molecular Therapy 29(12):3498—3511.
[19] Schlame, M., Towbin, J.A., Heerdt, P.M., Jehle, R., DiMauro, S., Blanck, T.J., 2002. Deficiency of tetralinoleoyl-cardiolipin in Barth syndrome. Annals of Neurology 51(5):634—637.
[20] Sparagna, G.C., Chicco, A.J., Murphy, R.C., Bristow, M.R., Johnson, C.A., Rees, M.L., et al., 2007. Loss of cardiac tetralinoleoyl cardiolipin in human and experimental heart failure. The Journal of Lipid Research 48(7):1559—1570.
[21] Hsu, P., Shi, Y., 2017. Regulation of autophagy by mitochondrial phospholipids in health and diseases. Biochimica et Biophysica Acta (BBA) - Molecular and Cell Biology of Lipids 1862(1):114—129.
[22] Hsu, P., Liu, X., Zhang, J., Wang, H.G., Ye, J.M., Shi, Y., 2015. Cardiolipin remodeling by TAZ/tafazzin is selectively required for the initiation of mitophagy. Autophagy 11(4):643—652.
[23] Zhang, J., Liu, X., Nie, J., Shi, Y., 2022. Restoration of mitophagy ameliorates cardiomyopathy in Barth syndrome. Autophagy, 1—16.
[24] Li, J., Romestaing, C., Han, X., Li, Y., Hao, X., Wu, Y., et al., 2010. Cardiolipin remodeling by ALCAT1 links oxidative stress and mitochondrial dysfunction to obesity. Cell Metabolism 12(2):154—165.
[25] Liu, X., Ye, B., Miller, S., Yuan, H., Zhang, H., Tian, L., et al., 2012. Ablation of ALCAT1 mitigates hypertrophic cardiomyopathy through effects on oxidative stress and mitophagy. Molecular and Cellular Biology 32(21):4493—4504.
[26] Wang, L., Liu, X., Nie, J., Zhang, J., Kimball, S.R., Zhang, H., et al., 2015. ALCAT1 controls mitochondrial etiology of fatty liver diseases, linking defective mitophagy to steatosis. Hepatology 61(2):486—496.
[27] Tyurina, Y.Y., Polimova, A.M., Maciel, E., Tyurin, V.A., Kapralova, V.I., Winnica, D.E., et al., 2015. LC/MS analysis of cardiolipins in substantia nigra and plasma of rotenone-treated rats: implication for mitochondrial dysfunction in Parkinson's disease. Free Radical Research 49(5):681—691.
[28] Gaudioso, A., Garcia-Rozas, P., Casarejos, M.J., Pastor, O., Rodriguez-Navarro, J.A., 2019. Lipidomic alterations in the mitochondria of aged parkin null mice relevant to autophagy. Frontiers in Neuroscience 13:329.
[29] Song, C., Zhang, J., Qi, S., Liu, Z., Zhang, X., Zheng, Y., et al., 2019. Cardiolipin remodeling by ALCAT1 links mitochondrial dysfunction to Parkinson's diseases. Aging Cell 18(3):e12941.
[30] Chaves-Filho, A.B., Pinto, I.F.D., Dantas, L.S., Xavier, A.M., Inague, A., Faria, R.L., et al., 2019. Alterations in lipid metabolism of spinal cord linked to amyotrophic lateral sclerosis. Scientific Reports 9(1):11642.
[31] Kirkinezos, I.G., Bacman, S.R., Hernandez, D., Oca-Cossio, J., Arias, L.J., Perez-Pinzon, M.A., et al., 2005. Cytochrome c association with the inner mitochondrial membrane is impaired in the CNS of G93A-SOD1 mice. Journal of Neuroscience 25(1):164—172.
[32] Bozzo, F., Mirra, A., Carri, M.T., 2017. Oxidative stress and mitochondrial damage in the pathogenesis of ALS: new perspectives. Neuroscience Letters 636:3—8.
[33] Cao, J., Liu, Y., Lockwood, J., Burn, P., Shi, Y., 2004. A novel cardiolipin-remodeling pathway revealed by a gene encoding an endoplasmic reticulum-associated acyl-CoA:lysocardiolipin acyltransferase (ALCAT1) in mouse. Journal of Biological Chemistry 279(30):31727—31734.
[34] Joshi, A.U., Saw, N.L., Vogel, H., Cunnigham, A.D., Shamloo, M., Mochly-Rosen, D., 2018. Inhibition of Drp1/Fis1 interaction slows progression of amyotrophic lateral sclerosis. EMBO Molecular Medicine 10(3).
[35] Osto, C., Benador, I.Y., Ngo, J., Liesa, M., Stiles, L., Acin-Perez, R., et al., 2020. Measuring mitochondrial respiration in previously frozen biological samples. Current Protocols in Cell Biology 89(1):e116.
[36] Zhang, X., Zhang, J., Sun, H., Liu, X., Zheng, Y., Xu, D., et al., 2019. Defective phosphatidylglycerol remodeling causes hepatopathy, linking mitochondrial dysfunction to hepatosteatosis. Cell Mol Gastroenterol Hepatol 7(4):763—781.
[37] Sun, J., Mu, Y., Jiang, Y., Song, R., Yi, J., Zhou, J., et al., 2018. Inhibition of p70 S6 kinase activity by A77 1726 induces autophagy and enhances the degradation of superoxide dismutase 1 (SOD1) protein aggregates. Cell Death & Disease 9(3):407.
[38] Al-Sarraj, S., King, A., Cleveland, M., Pradat, P.F., Corse, A., Rothstein, J.D., et al., 2014. Mitochondrial abnormalities and low grade inflammation are present in the skeletal muscle of a minority of patients with amyotrophic lateral sclerosis; an observational myopathology study. Acta Neuropathol Commun 2:165.
[39] Papadeas, S.T., Kraig, S.E., O'Banion, C., Lepore, A.C., Maragakis, N.J., 2011. Astrocytes carrying the superoxide dismutase 1 (SOD1G93A) mutation induce wild-type motor neuron degeneration in vivo. Proceedings of the

National Academy of Sciences of the United States of America 108(43): 17803–17808.
[40] Komine, O., Yamanaka, K., 2015. Neuroinflammation in motor neuron disease. Nagoya Journal of Medical Science 77(4):537–549.
[41] Brites, D., Vaz, A.R., 2014. Microglia centered pathogenesis in ALS: insights in cell interconnectivity. Frontiers in Cellular Neuroscience 8:117.
[42] Jaarsma, D., Rognoni, F., van Duijn, W., Verspaget, H.W., Haasdijk, E.D., Holstege, J.C., 2001. CuZn superoxide dismutase (SOD1) accumulates in vacuolated mitochondria in transgenic mice expressing amyotrophic lateral sclerosis-linked SOD1 mutations. Acta Neuropathologica 102(4):293–305.
[43] Liu, J., Lillo, C., Jonsson, P.A., Vande Velde, C., Ward, C.M., Miller, T.M., et al., 2004. Toxicity of familial ALS-linked SOD1 mutants from selective recruitment to spinal mitochondria. Neuron 43(1):5–17.
[44] Liu, H.N., Tjostheim, S., Dasilva, K., Taylor, D., Zhao, B., Rakhit, R., et al., 2012. Targeting of monomer/misfolded SOD1 as a therapeutic strategy for amyotrophic lateral sclerosis. Journal of Neuroscience 32(26):8791–8799.
[45] Sheng, Y., Chattopadhyay, M., Whitelegge, J., Valentine, J.S., 2012. SOD1 aggregation and ALS: role of metallation states and disulfide status. Current Topics in Medicinal Chemistry 12(22):2560–2572.
[46] Puttaparthi, K., Wojcik, C., Rajendran, B., DeMartino, G.N., Elliott, J.L., 2003. Aggregate formation in the spinal cord of mutant SOD1 transgenic mice is reversible and mediated by proteasomes. Journal of Neurochemistry 87(4): 851–860.
[47] Furukawa, Y., O'Halloran, T.V., 2005. Amyotrophic lateral sclerosis mutations have the greatest destabilizing effect on the apo- and reduced form of SOD1, leading to unfolding and oxidative aggregation. Journal of Biological Chemistry 280(17):17266–17274.
[48] Chao, H., Anthonymuthu, T.S., Kenny, E.M., Amoscato, A.A., Cole, L.K., Hatch, G.M., et al., 2018. Disentangling oxidation/hydrolysis reactions of brain mitochondrial cardiolipins in pathogenesis of traumatic injury. JCI insight 3(21):e97677.
[49] Monteiro-Cardoso, V.F., Oliveira, M.M., Melo, T., Domingues, M.R., Moreira, P.I., Ferreiro, E., et al., 2015. Cardiolipin profile changes are associated to the early synaptic mitochondrial dysfunction in Alzheimer's disease. Journal of Alzheimer's Disease 43(4):1375–1392.
[50] Cheng, H., Mancuso, D.J., Jiang, X., Guan, S., Yang, J., Yang, K., et al., 2008. Shotgun lipidomics reveals the temporally dependent, highly diversified cardiolipin profile in the mammalian brain: temporally coordinated postnatal diversification of cardiolipin molecular species with neuronal remodeling. Biochemistry 47(21):5869–5880.
[51] Bruijn, L.I., Houseweart, M.K., Kato, S., Anderson, K.L., Anderson, S.D., Ohama, E., et al., 1998. Aggregation and motor neuron toxicity of an ALS-linked SOD1 mutant independent from wild-type SOD1. Science 281(5384): 1851–1854.
[52] Cleveland, D.W., Liu, J., 2000. Oxidation versus aggregation - how do SOD1 mutants cause ALS? Nature Medicine 6(12):1320–1321.
[53] Williamson, T.L., Corson, L.B., Huang, L., Burlingame, A., Liu, J., Bruijn, L.I., et al., 2000. Toxicity of ALS-linked SOD1 mutants. Science 288(5465):399.
[54] Agorogiannis, E.I., Agorogiannis, G.I., Papadimitriou, A., Hadjigeorgiou, G.M., 2004. Protein misfolding in neurodegenerative diseases. Neuropathology and Applied Neurobiology 30(3):215–224.
[55] Kokubo, Y., Taniguchi, A., Hasegawa, M., Hayakawa, Y., Morimoto, S., Yoneda, M., et al., 2012. alpha-Synuclein pathology in the amyotrophic lateral sclerosis/parkinsonism dementia complex in the Kii Peninsula, Japan. Journal of Neuropathology and Experimental Neurology 71(7):625–630.
[56] Watanabe, M., Dykes-Hoberg, M., Culotta, V.C., Price, D.L., Wong, P.C., Rothstein, J.D., 2001. Histological evidence of protein aggregation in mutant SOD1 transgenic mice and in amyotrophic lateral sclerosis neural tissues. Neurobiology of Disease 8(6):933–941.
[57] Mattiazzi, M., D'Aurelio, M., Gajewski, C.D., Martushova, K., Kiaei, M., Beal, M.F., et al., 2002. Mutated human SOD1 causes dysfunction of oxidative phosphorylation in mitochondria of transgenic mice. Journal of Biological Chemistry 277(33):29626–29633.
[58] Magrane, J., Hervias, I., Henning, M.S., Damiano, M., Kawamata, H., Manfredi, G., 2009. Mutant SOD1 in neuronal mitochondria causes toxicity and mitochondrial dynamics abnormalities. Human Molecular Genetics 18(23): 4552–4564.
[59] Peng, J., Pan, J., Mo, J., Peng, Y., 2022. MPO/HOCl facilitates apoptosis and ferroptosis in the SOD1(G93A) motor neuron of amyotrophic lateral sclerosis. Oxidative Medicine and Cellular Longevity 2022:8217663.
[60] Philips, T., Robberecht, W., 2011. Neuroinflammation in amyotrophic lateral sclerosis: role of glial activation in motor neuron disease. The Lancet Neurology 10(3):253–263.
[61] Roberts, K., Zeineddine, R., Corcoran, L., Li, W., Campbell, I.L., Yerbury, J.J., 2013. Extracellular aggregated Cu/Zn superoxide dismutase activates microglia to give a cytotoxic phenotype. Glia 61(3):409–419.
[62] Oono, M., Okado-Matsumoto, A., Shodai, A., Ido, A., Ohta, Y., Abe, K., et al., 2014. Transglutaminase 2 accelerates neuroinflammation in amyotrophic lateral sclerosis through interaction with misfolded superoxide dismutase 1. Journal of Neurochemistry 128(3):403–418.
[63] Miller, D.W., Cookson, M.R., Dickson, D.W., 2004. Glial cell inclusions and the pathogenesis of neurodegenerative diseases. Neuron Glia Biology 1(1):13–21.
[64] Boillee, S., Yamanaka, K., Lobsiger, C.S., Copeland, N.G., Jenkins, N.A., Kassiotis, G., et al., 2006. Onset and progression in inherited ALS determined by motor neurons and microglia. Science 312(5778):1389–1392.
[65] Wang, L., Gutmann, D.H., Roos, R.P., 2011. Astrocyte loss of mutant SOD1 delays ALS disease onset and progression in G85R transgenic mice. Human Molecular Genetics 20(2):286–293.
[66] Gugliandolo, A., Giacoppo, S., Bramanti, P., Mazzon, E., 2018. NLRP3 inflammasome activation in a transgenic amyotrophic lateral sclerosis model. Inflammation 41(1):93–103.
[67] Jaiswal, M.K., 2019. Riluzole and edaravone: a tale of two amyotrophic lateral sclerosis drugs. Medicinal Research Reviews 39(2):733–748.
[68] Borras-Blasco, J., Plaza-Macias, I., Navarro-Ruiz, A., Peris-Marti, J., Anton-Cano, A., 1998. [Riluzole as a treatment for amyotrophic lateral sclerosis]. Revue Neurologique 27(160):1021–1027.

